Silicon (2023) 15:7523–7540
https://doi.org/10.1007/s12633-023-02528-x

RESEARCH

Preparation and Characterization of UV-Enhanced GaN/ Porous Si Photodetector using PLA in Liquid

Makram A. Fakhri[1] · Ali A. Alwahib[1] · Evan T. Salim[2] · Raid A. Ismail[2] · Husam Aldin A. Abdul Amir[1] · Raed Khalid Ibrahim[3] · Sarmad Fawzi Hamza Alhasan[4] · Forat H. Alsultany[5] · Zaid T. Salim[6] · Subash C. B. Gopinath[6,7,8]

Received: 22 March 2023 / Accepted: 20 May 2023 / Published online: 24 July 2023

Abstract
The photoluminescence and optoelectronics properties are very important for gallium nitride (GaN) nanoparticles in the applications of ultraviolet and blue optoelectronic devices. In this article, GaN nanoparticles are prepared and fabricated using femtosecond pulse laser ablation in liquid (PLAL). The X-ray diffraction results confirm that the synthesized GaN NPs are crystalline with a mixture of cubic and hexagonal phases, and the nanoparticles synthesized at 532 nm exhibit better crystallinity. The field emission electron microscope (FE-SEM) results demonstrate that the porous silicon consists of a high concentration of semicircular pores with an average diameter of the pore around 20 µm. Furthermore, the optoelectronic properties of the GaN/PSi are investigated to confirm its feasibility for double-junction photodetector and its applications. The outcomes show that the maximum responsivity was 3.8 A/W at 330 nm for a photodetector fabricated at 532 nm laser wavelength.

Keywords Gallium nitride · Nanoparticles · Laser ablation · Liquid · Porous silicon · Photodetector

1 Introduction

Gallium nitride (GaN) is one of the most important semiconducting materials of groups III-nitride, which has been employed in various industrial and technological applications due to its excellent optical and electrical properties, for example, optoelectronic devices, electronic devices, biosensors, chemical sensors [1–6]. GaN has a direct energy gap and high saturation velocity of $Vs = 2.7 \times 10^7$ cm/s, indicating it can be certainly well suited for the fabrication of UV photodetectors [7, 8]. Additionally, GaN has high thermal stability, radiation hardness, and excellent tolerability in harsh environments [9, 10]. Combining GaN-based devices with Si-based microelectronics is another possible advantage associated with the future of Si substrates [11, 12]. This type of combination can potentially be applied with those of highly advanced Si electronic devices by the hetero-epitaxial system of GaN on the Si substrate [13–15]. Either polycrystalline growth or a significant diffusion of Si into the GaN film results in the direct growth of a GaN film on the Si substrate [16, 17].

Various methods were employed to prepare GaN such as molecular beam epitaxy (MBE)[18, 19], metal–organic

✉ Makram A. Fakhri
mokaram_76@yahoo.com;
makram.a.fakhri@uotechnology.edu.iq

✉ Evan T. Salim
evan.t.salim@uotechnology.edu.iq; evan_tarq@yahoo.com

1 Laser and Optoelectronic Department, University of Technology-Iraq, Baghdad, Iraq

2 Applied Science Department, University of Technology-Iraq, Baghdad, Iraq

3 Al-Farahidi University, Baghdad, Iraq

4 Department of Communication Engineering, University of Technology-Iraq, Baghdad, Iraq

5 Department of Medical Physics, Al-Mustaqbal University College, Baghdad, Iraq

6 Institute of Nano Electronic Engineering, Universiti Malaysia Perlis (UniMAP), 01000 Kangar, Perlis, Malaysia

7 Faculty of Chemical Engineering & Technology, Universiti Malaysia Perlis (UniMAP), 02600 Arau, Perlis, Malaysia

8 Micro System Technology, Centre of Excellence (CoE), Universiti Malaysia Perlis (UniMAP), Pauh Campus, 02600 Arau, Perlis, Malaysia

chemical vapor deposition (MOCVD) [20–22], pulsed laser deposition (PLD) [23–28], chemical vapor deposition (CVD), pulsed laser ablation (PLA) [29–33]. Pulsed laser ablation in liquid (PLAL) is considered one of the attractive routes to the synthesis of nanoparticles [34, 35]. It exhibits many advantages such as simplicity, low cost, no vacuum needed, production of nanoparticles with different morphologies, and high purity products [36–38].

Herein, we report the preparation of GaN nanoparticles by laser ablation in liquid at laser wavelengths of 532 and 1064 nm. The aim of the work is to fabricate high-quality gallium nitride (GaN) nanoparticles (NPs) using pulsed laser ablation technology and deposit them on porous Si substrates at two different wavelengths for the pulsed laser. The uniqueness of the work being reported is that liquid ethanol was employed as a cooling liquid to keep the nanoparticle from oxidizing after liquid GaN nanoparticle was initially created by pulsed laser ablation in liquid from bulk GaN. Finally, the Fabrication and characterization of UV-enhanced GaN/porous silicon double-junction photodetectors is the third objective of this work.

2 Experimental Setup

Colloidal GaN nanoparticles were synthesized by pulsed Nd: YAG laser ablation of GaN target immersed in 10 ml ethanol, as shown in Fig. 1. The ablation was performed at two laser wavelengths; 532 and 1064 nm. This laser source has pulse duration of 7 ns, pulse repetition frequency of 1 Hz, and laser fluence of 1.J/cm^2. The number of laser pulses was 1000 for each wavelength and the laser beam was focused at the target using a converging lens with a focal length of 12 cm.

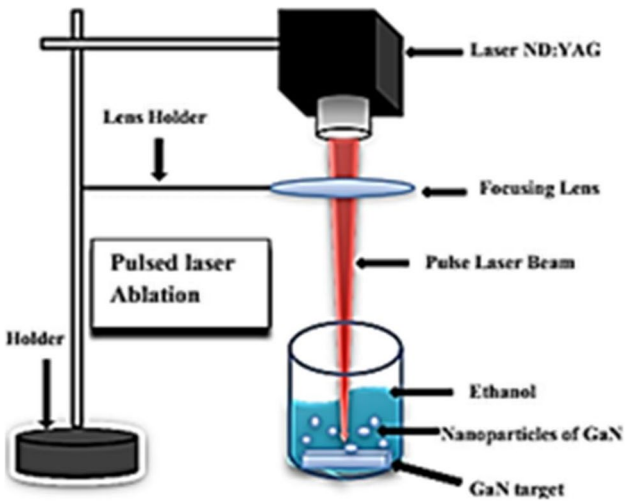

Fig. 1 Schematic diagram of laser ablation in liquid system

Filmetrics F20 optical reflectometer has been used to measure the thickness and reflectivity of the prepared samples. The UV–Visible spectrophotometer (Shimadzu 1800) was employed to measure the optical properties of GaN film deposited on the glass substrate. Photoluminescence properties were investigated using Jobin Yvon model spectroscopy HR 800 UV employing He-Cd laser with 352 nm wavelength. The structural properties of the GaN NPs were investigated using a high-resolution X-ray diffractometer (Panalytical Company, Netherlands). The morphological properties of the nanoparticles have been studied using a field emission scanning electron microscope (FESEM) (FEI/Nova Nano SEM450). Atomic force microscopy (AFM) was used to study the topography of the nanoparticles and measure the roughness of GaN nanostructures. The n-type porous silicon was used as a substrate in this study. The porous silicon was prepared by laser–assisted electrochemical etching. The etching was carried out by immersing the single-crystal silicon substrate in Teflon container with a 20 ml HF (48%) solution. The gold rod and DC power supply were connected to the Teflon base through the metal side and to the gold rod immersed in the HF solution at a current (60 mA) for 10 min. A diode laser with wavelength (650 nm) and power of (30 mW) was used for the illumination through the etching process. The schematic diagram of the laser-assisted electrochemical etching process and porous silicon image are depicted in Fig. 2(a, & b).

The colloidal GaN nanomaterials were deposited on the porous silicon by a drop-casting method, as shown in Fig. 3. The porous silicon substrate was heated by a hot plate at a temperature of 70 °C. Each drop on the porous silicon substrate was left drying and then followed by another drop reaching 100 drops to form the thin film of the GaN on the porous silicon substrate. All the processes were taken around 12 h to avoid oxidation. The colloidal nanoparticle was adequately shaken before each drop to keep the GaN nanomaterials with minim agglomeration.

A vacuum evaporation system is used to deposit aluminum (Al) on the GaN/ Porous Silicon-n (111) surface to form ohmic contact electrodes through a specially designed interdigit Al mask as depicted in Fig. 4. The I-V characteristics in the dark and illumination conditions were investigated using the DF LT30/2 Power Supply, (UNI-T-UT33C), and digital multimeters (TEKR. CDM 250). The capacitance–voltage C-V characteristics were measured using a programmable RCL meter from (Fluke PM6306). An optical monochromator was used to measure the spectral responsivity of the GaN/PSi double-junction photodetector in the spectral reign of (200 nm–900 nm). All the tests were carried out at room temperature.

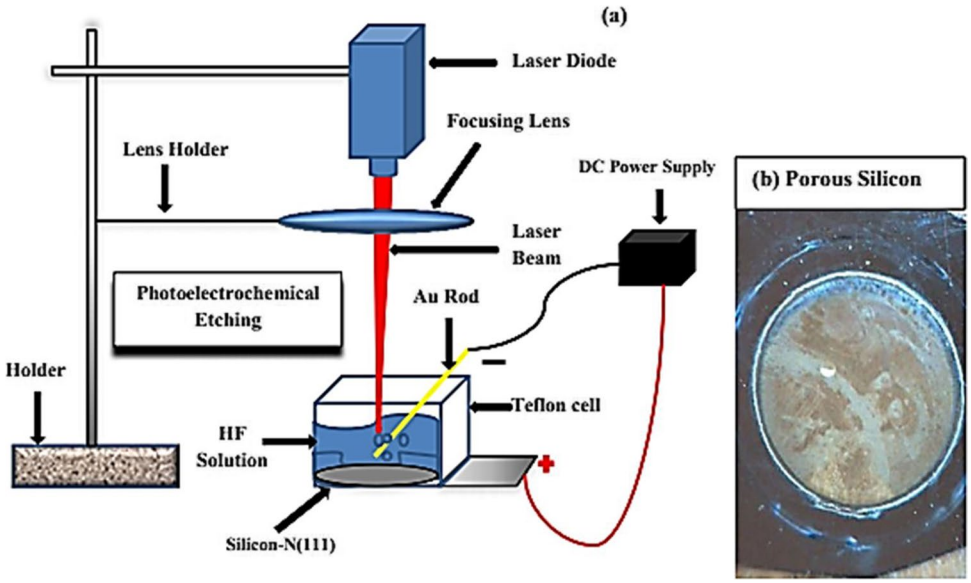

Fig. 2 (**a**) Laser-assisted electrochemical etching system and (**b**) Photograph of porous Silicon

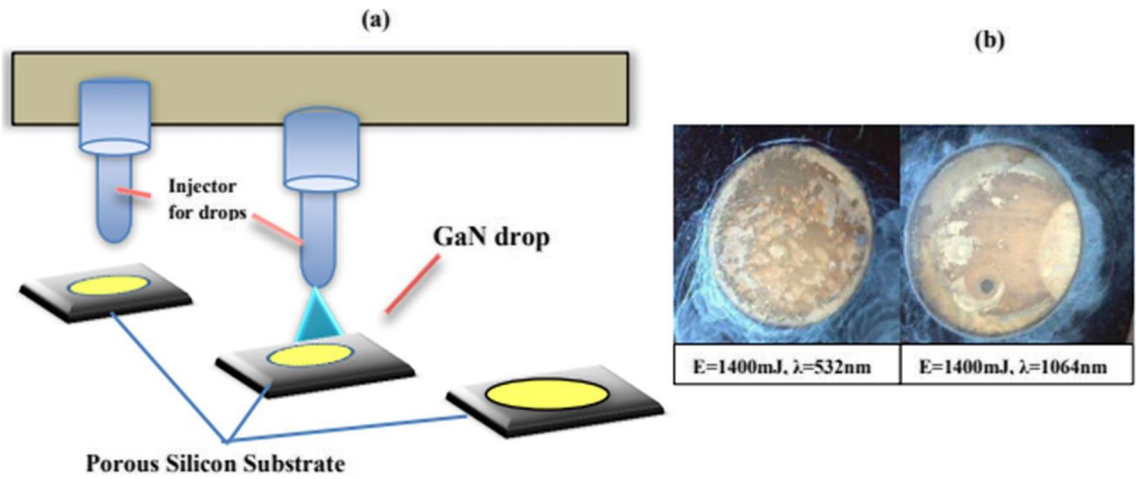

Fig. 3 (**a**) Schematic diagram of drop-casting method (**b**) Photographs of GaN/ Porous Silicon prepared at two laser wavelengths

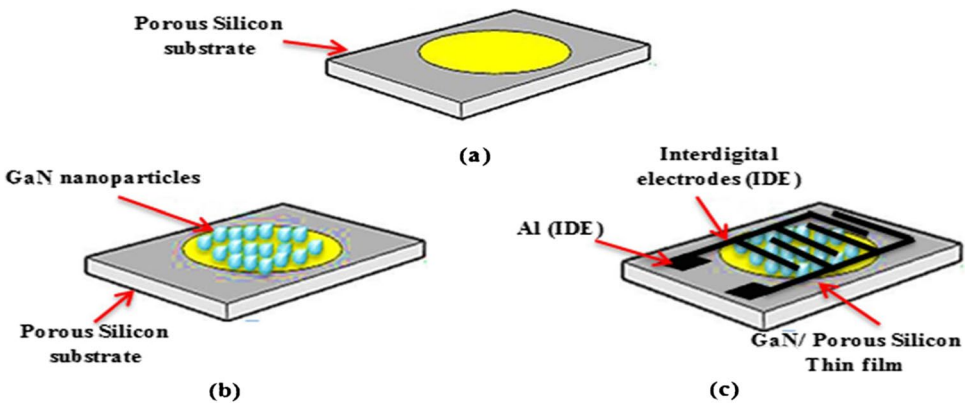

Fig. 4 Schematic illustration of preparation of the photodetector (**a**) Porous Silicon-n (111) substrate, (**b**) Preparation of GaN/ Porous Silicon-n (111), and (**c**) Ohmic contact deposition

3 Results and Discussions

3.1 Structural Properties

Figure 5 presents the XRD patterns of nanoporous Silicon and GaN nanoparticles. The GaN nanoparticles were presented at both ablation wavelengths of 532 nm and 1064 nm in ethanol and drop-casted on the prepared porous silicon substrate. Figure 5a shows a sharp peak of the porous silicon XRD patterns at $2\theta = 28.74°$ corresponding to the (111) plane. Figure 5b presents the XRD pattern of GaN nanoparticles prepared at the wavelength of 532 nm; it exhibits a mixed structure of hexagonal h-GaN phase and cubic phase c-GaN. The h-GaN phase was observed at $2\theta = 34.54°$ and 37.49° corresponded to (002) and (101), respectively, while the c-GaN phase

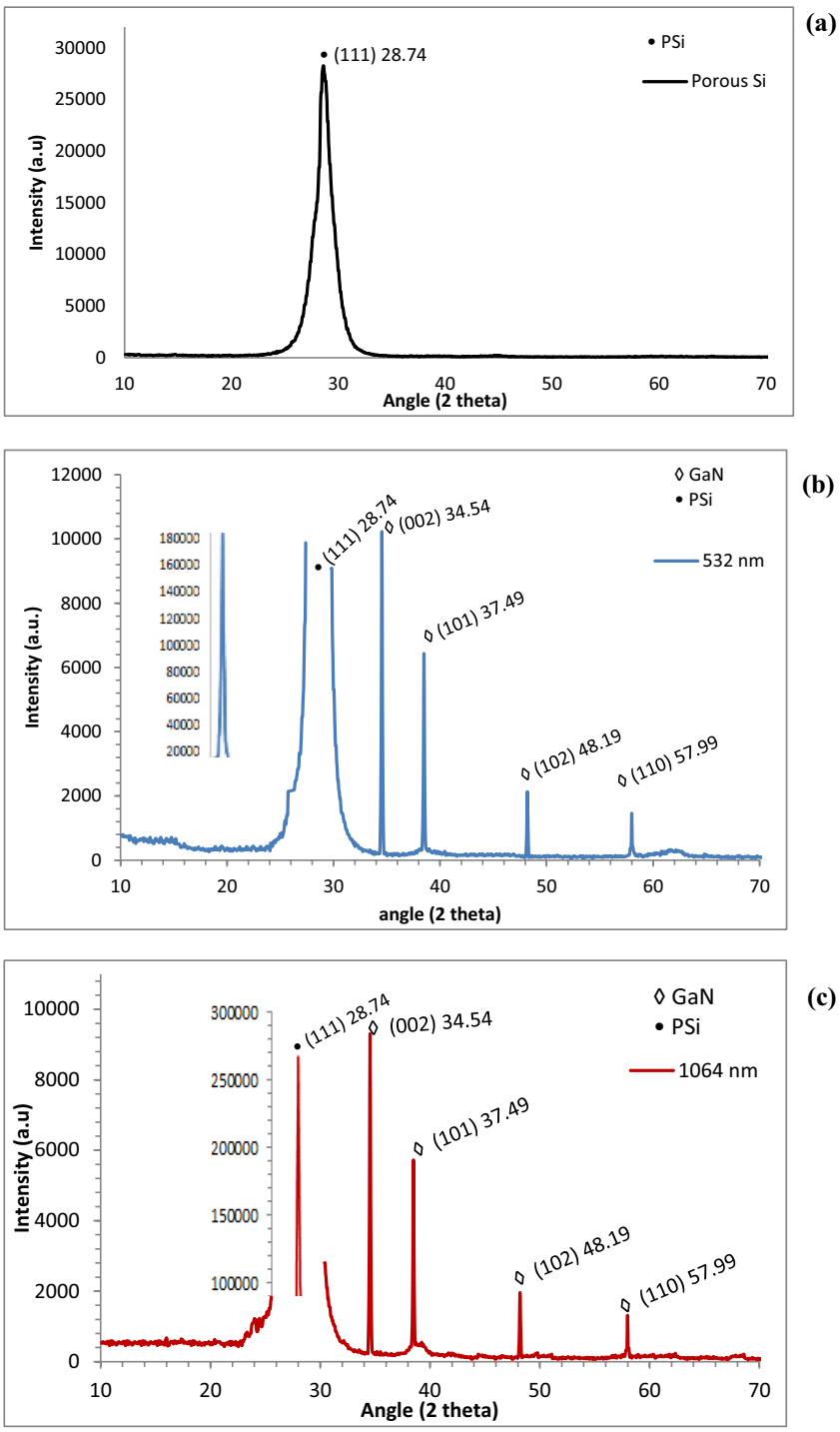

Fig.5 XRD patterns of (**a**) the porous Silicon, (**b**) GaN nanoparticles prepared at 532 nm), and (**c**) GaN nanoparticles synthesized at 1064 nm

was detected at 2θ = 48.19° and 2θ = 57.99°, which corresponded to (102) and (110), respectively. These XRD peaks are matched with JCPDs#2–1078 and 82,364 for h-GaN and c-GaN, respectively [39–41]. Figure 5c presents the XRD pattern of GaN nanoparticles prepared at 1064 nm. As shown, Fig. 5c shows the presence of the three peaks located at 2θ = 34.54°, 37.49, 48.19°, and 57.99°, which corresponded to (002), (101), (102), (110) planes, respectively, which belonged to h-GaN and c-GaN phases. Compared to the sample prepared at 532 nm wavelength, the sample prepared at 1064 nm shows less intensity and less sharpness indicating a low degree of crystallinity [42–44]. This result can be ascribed to the fact that the absorption coefficient of 52 nm laser wavelength is higher than that of 1064 nm, indicating the formation of a smaller absorption depth and the ablated nanoparticles and monodispersed and grown in high crystallization [45–48].

3.2 Morphological Properties

3.2.1 AFM Results

Figure 6-a illustrates the 3D AFM images of the porous silicon and GaN nanoparticles prepared with 532 and 1064 nm. The AFM image of porous silicon reveals the formation of circular pores distributed uniformly over the surface. The root means square RMS of surface roughness and pore size were 8.9 and 53 nm, respectively. The 3D AFM images of CaN NPs prepared at 532 and 1064 nm are shown in Fig. 6-b&c. We can see clearly that the pours layers are completely covered and the pores are filled with GaN NPs. The grain size of the prepared nanofilms (GaN) that were proven in the AFM test is consistent with the crystallite size that was calculated from the XRD results [49, 50]. The RMS of surface roughness of the porous silicon filled with GaN NPs prepared at 532 and 1064 nm were 8.8 and 25.1 nm, respectively. The large surface roughness of porous covered with GaN NPs prepared at 1064 nm can be attributed to the large particle size that comes from the agglomeration effect as well as the high concentration of GaN NPs produced by 1064 nm laser pulses, this result is consistent with the reported results [47–50]. Table 1 lists the RMS of surface roughness and grain size of GaN NPs synthesized at 532 and 1064 nm.

Figure 7 represents the relation between the grain's density and the grain's size at different ablation wavelengths. The first porous silicon sample exhibits average grain size (39.3 nm) with grain density (0.0035). The selection of work at 532 nm presents the average smallest grain size of (26.1) with the highest grain density due to high regular crystal distribution and back to decrease at the sample of 1064 nm because of the decrease in the regularity of the crystal distribution [51, 52]. The surface topography of GaN nanophotonic as observed from the AFM micrographs proves that the grains are uniformly distributed within the scanning area (78 nm × 78 nm), with individual columnar grains extending upward. This surface characteristic was quoted from the topographic image, which is uniform, smooth, and homogeneous at 532 nm due to the excellent quality of the structure crystallization.

3.2.2 FESEM Results

Figure 8 presents the top view FESEM images of porous silicon and GaN deposited on porous silicon. As shown in Fig. 8-a, the porous silicon consists of high-density of circular shape pores having different sizes. The formation of large size pores is due to the coalescence of small pores which leads to form irregular pores as denoted by arrows. The average pore size of porous silicon was around 20 µm. The SEM image shown in Fig. 8-b illustrates the GaN nanoparticles covered in porous silicon prepared with 532 nm laser pulses. As shown, most of the nanoparticles are filled in the pores, while the other nanoparticles are deposited on the walls of the porous surface. Figure 8-c shows the SEM image of GaN nanoparticles deposited on the porous silicon synthesized at 1064 nm [53–55]. It is clearly seen that most porous are filled with GaN nanoparticles and only a few pores remained unfilled. This result can be attributed to the particle size and concentration of agglomerated GaN nanoparticles. The EDX spectrum of porous silicon exhibits a high peak of Si and a small peak of oxygen due to the trapping of oxygen atoms in pores. The EDX of GaN nanoparticles deposited on porous silicon shows the presence of peaks related to Ga and N with atomic percentage [Ga]/[N] ratios of 2.7 and 4.3 for samples prepared with 532 and 1064 nm, respectively [56–58]. The formation of incomplete stoichiometric GaN is due to the reaction of nitrogen with oxygen and formed NO2 gas. This occurred as a result of the instability of GaN nanoparticles. Figure 9 shows the TEM images of GaN nanoparticles prepared at 532 and 1064 nm.

The TEM images revealed the formation of spherical GaN nanoparticles with average particle sizes of 22 and 30 nm for samples prepared at 532 and 1064 nm, respectively. As shown in Fig. 9, the particle size of GaN prepared with 532 nm is smaller than that synthesized with 1064 nm due to the larger absorption depth of the laser with a wavelength of 1064 nm compared to that prepared with 532 nm [59, 60].

3.3 Optical Properties

3.3.1 UV–Visible Spectrophotometer

Figure 10 presents the UV–Vis optical reflectance spectra of PSi and GaN/PSi prepared at 532 and 1064 nm in the

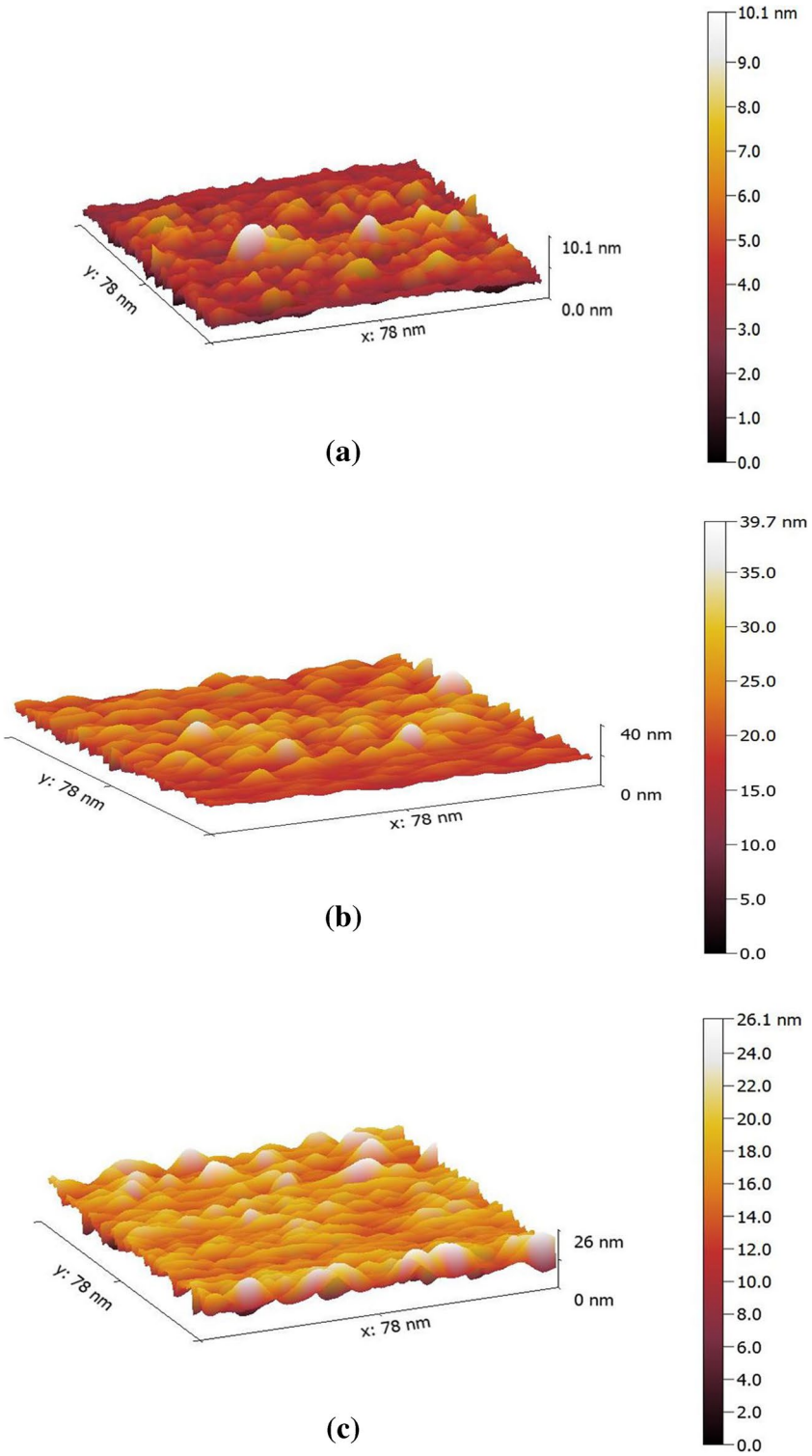

Fig.6 3DAFM images of (**a**) porous silicon, (**b**) GaN/PSi prepared at 532 nm and (**c**) GaN/PSi nanostructure prepared at the 1064 nm

spectral region of 300–900 nm. Figure 10 shows that the optical reflectance of GaN/PSi increases as laser wavelength increases and tends to saturate after 450 nm and after this wavelength increases sharply. The reflectance spectra of GaN prepared at two laser wavelengths increased with wavelength in the same manner but the reflectivity of GaN prepared at 1064 nm is slightly higher. As shown, an oscillation is detected as a result of the interference effect. The inset of Fig. 10 shows the reflectivity plot of the porous silicon surface. The reflectivity increases as the laser wavelength up to 520 nm and after that is saturated. The reflectivity is very low compared to that of GaN/PSi.

Table 1 AFM data of the porous silicon and the GaN/pSi nanostructures prepared at two 532 nm and 1064 nm

Samples	Laser ablation wavelength (nm)	Roughness (nm)	Root-mean-square value (nm)	Grain size (nm)
PSi	-	6.71	9.1	39.3
GaN/PSi	532	7.4	8.8	26.1
GaN/PSi	1064	21.6	25.1	53.2

Figure 11 presents the optical energy gap of the porous silicon substrates and GaN nanostructure grown on a porous silicon substrate at the wavelength of (532 nm) and (1064 nm). The Kubelka–Munk (K-M) function and Tauc plots were used to calculate the energy bandgap of the pSi and GaN nanostructure. F(R) was used in the K-M formula, where R is the reflectivity, as shown in the following equation [61–65].

$$F_{KM} = \frac{(1 - R^2)}{2R} \tag{1}$$

The degree of crystallization affects the band gap of GaN nanoparticles. The value of the energy gap of porous silicon was around 2.29, and 2.36 eV, while the energy gap of GaN prepared at 532 and 1064 nm was 3.6 and 3.75 eV, respectively. The slight increment in the energy gap of GaN can be attributed to the smaller nanoparticles obtained by 532 nm, which is consistent with the TEM investigation. The inset of Fig. 11 shows the optical band gap plot of the porous silicon surface.

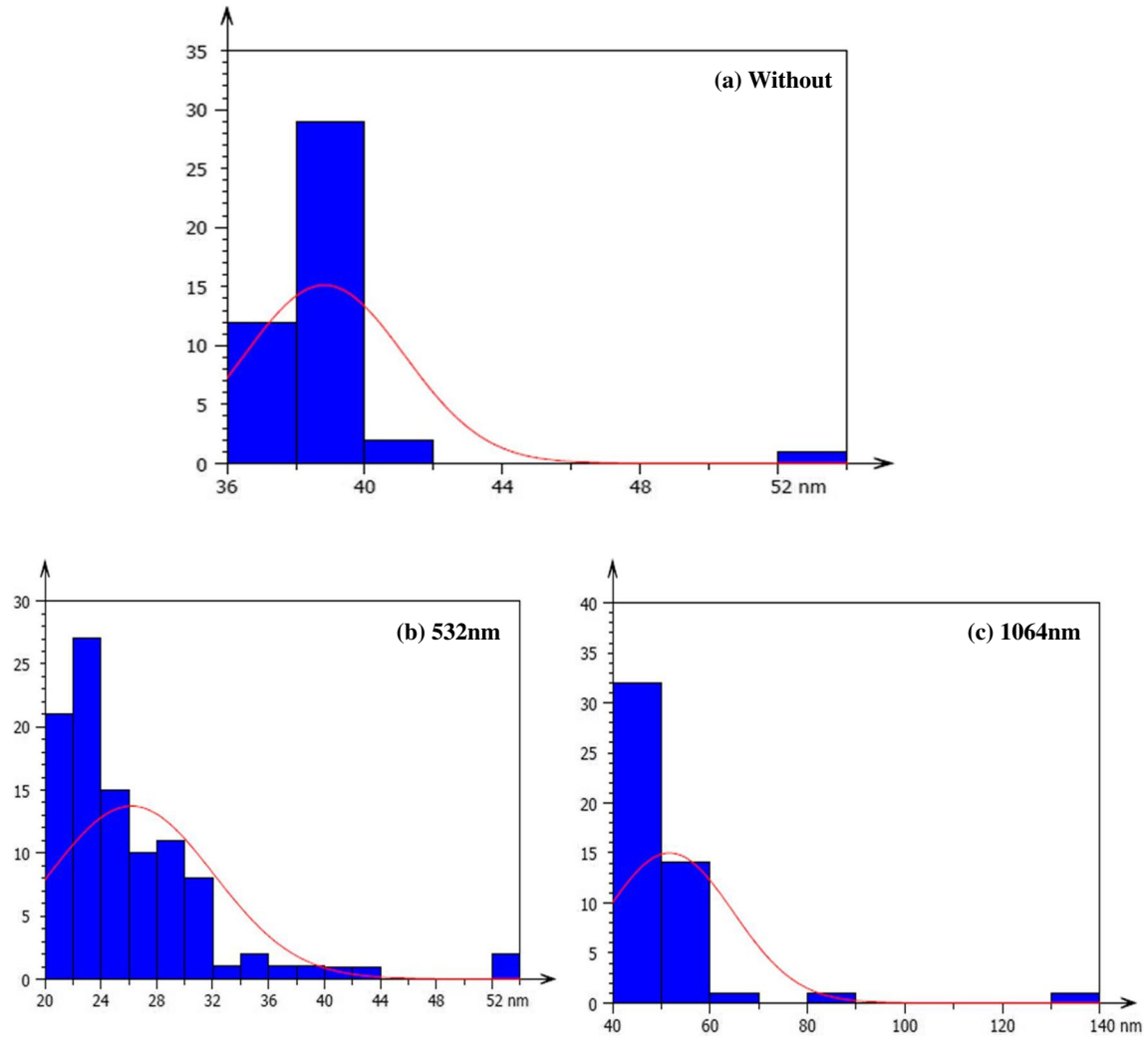

Fig. 7 The average grain size curve of (**a**) the porous Silicon, (**b**) GaN/pSi nanostructures at the wavelength (532 nm), and (**c**) GaN/pSi nanostructures at the wavelength (1064 nm)

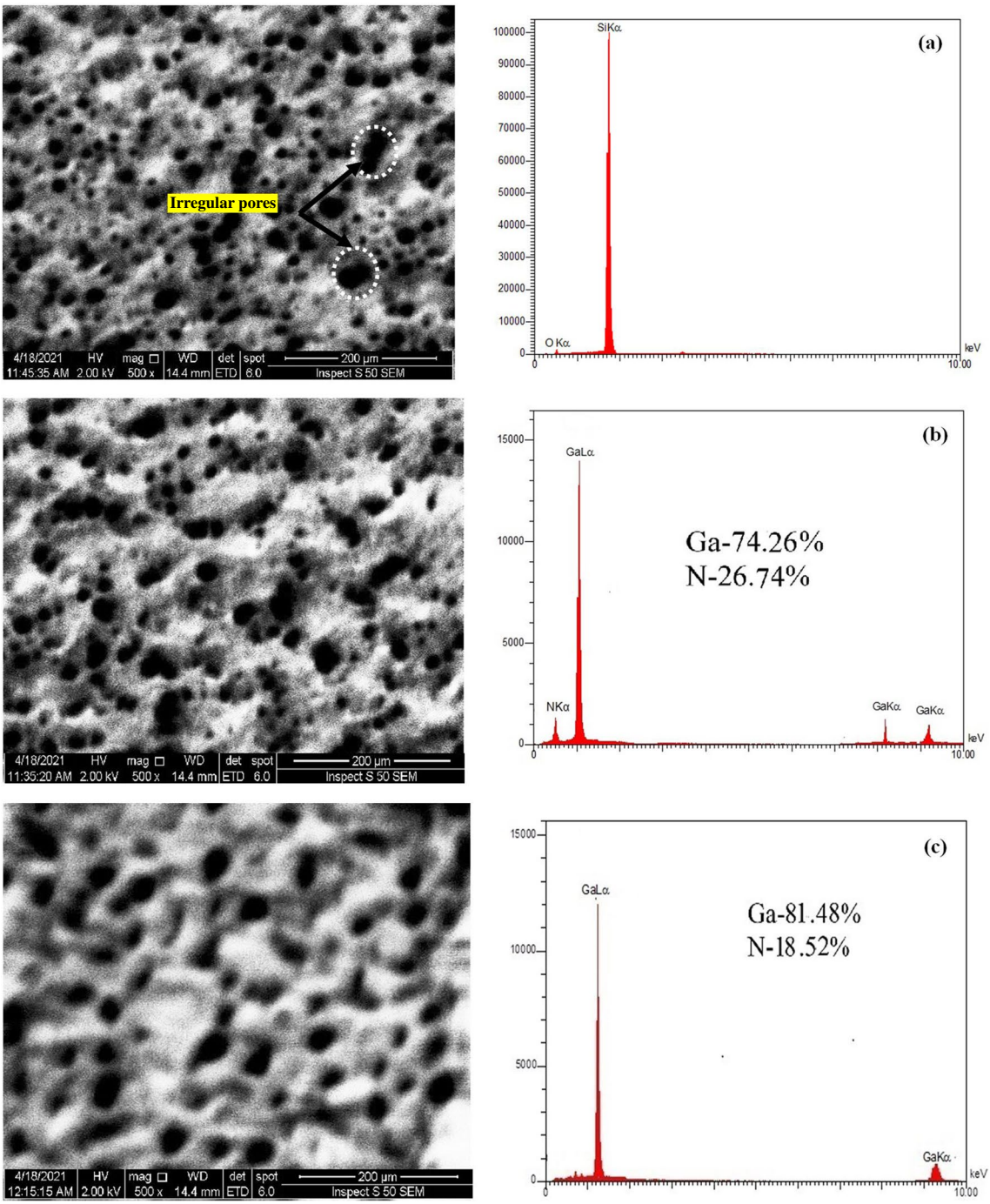

Fig. 8 The FESEM images and EDX spectra of (**a**) the porous Silicon, (**b**) GaN/pSi nanostructures at the wavelength (532 nm), and (**c**) GaN/pSi nanostructures at the wavelength (1064 nm)

3.3.2 Photoluminescence (PL)

The photoluminescence (PL) spectra of porous silicon substrates and GaN nanostructure grown on a porous silicon substrate at the wavelength of 532 nm and 1064 nm are shown in Fig. 12 demonstrate. The porous silicon presents a single peak located at 640 nm (1.94 eV). The sample synthesized at 532 nm exhibits two PL peaks, a high-intensity UV peak located at 321 nm (3.86 eV), and a second peak detected at 640 nm (1,94 eV). The first peak has belonged to the band-to-band GaN which is in good agreement with the energy gap determined from UV–Vis absorption and the second peak is related to porous silicon. A small blue shift in the PL peak was

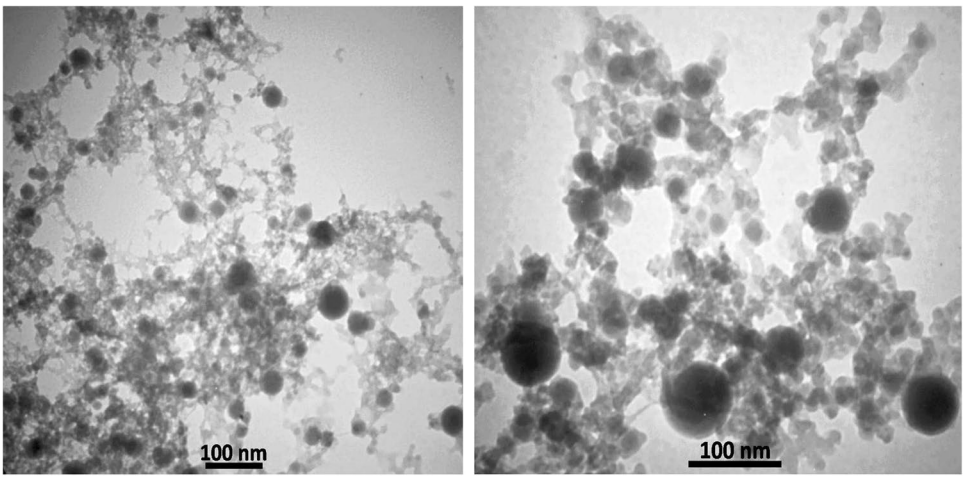

Fig. 9 TEM images of GaN nanoparticles synthesized at (left) 532 nm and (right) 106 nm

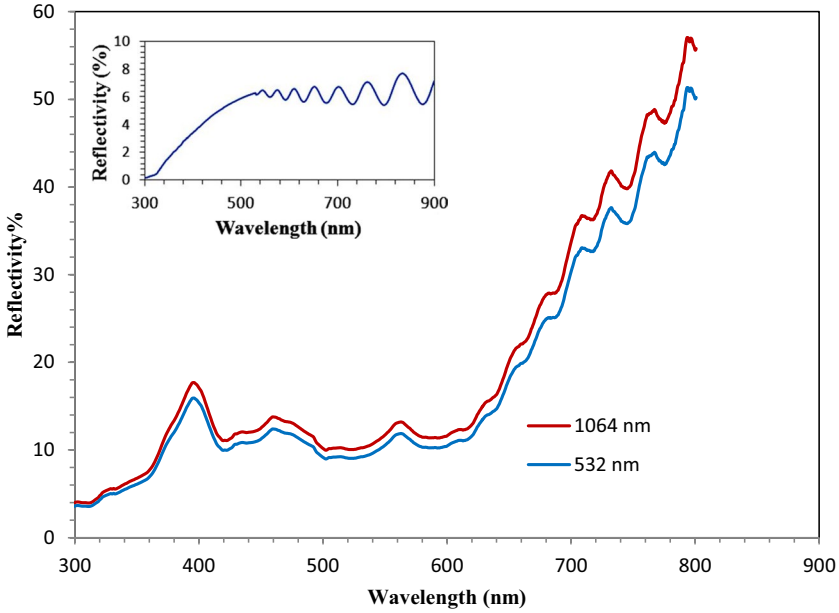

Fig.10 Reflectance diagram of GaN nanostructure grown on a porous silicon substrate at the wavelength of (532 nm), (1064 nm), and pSi substrates (inset)

observed for sample prepared at 532 nm due to the small nanoparticles [66–69].

The photoluminescence results also showed a variation in the peak intensity values, where the highest peak intensity of the porous silicon was at the base of the pure porous silicon without the gallium nitride layer, and this is very logical as the examination and absorption will be completely concentrated on the surface of the porous silicon. When examining the porous silicon base on which gallium nitride was deposited on top, it showed that the peak intensity value at 532 nm is higher than the peak intensity value at 1064 nm as a result of the highest crystallinity and the surface is also more regular and the best distribution and smooth [70–72].

3.4 Optoelectronic Properties of GaN/PSi Heterojunction Photodetector

Figure 13 shows the dark (I-V) characteristics of PSi/c-Si and GaN/PSi heterojunctions at room temperature in the range of applied voltage (−5 to +5 V). All the samples exhibit a rectification, which depends on the preparation condition. In three samples, the forward current increases with bias voltage. The highest forward current was found for GaN/PSi prepared at 532 nm. The forward current of GaN/PSi heterojunctions increases exponentially with voltage which agrees with that for aniso-type heterojunctions. Increasing the forward current of PSi/c-Si after being deposited with GaN nanoparticles is due to decreasing the electrical resistivity

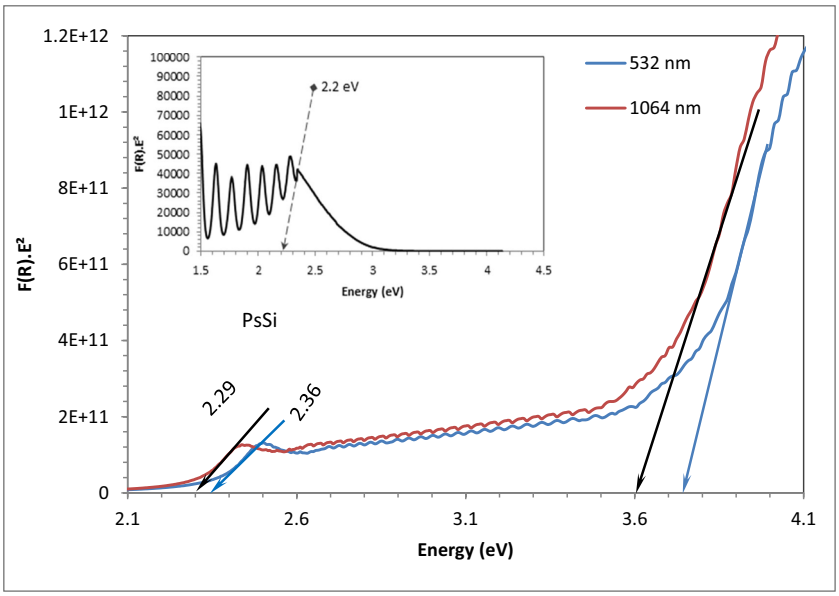

Fig. 11 Optical energy bandgap diagram of GaN nanostructure grown on a porous silicon substrate at the wavelength of (532 nm), (1064 nm), and pSi substrates (inset)

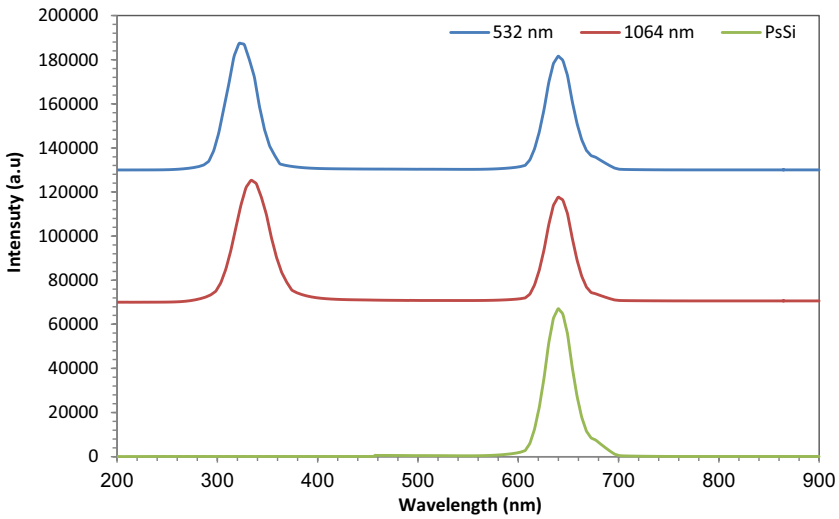

Fig. 12 PL spectra of GaN at different laser ablation wavelength

as well as the formation of double junctions, namely, GaN/PSi and PSi/c-Si. [73–75]. On the other hand, the reverse current of GaN/Si heterojunction was found to be voltage independent, while it increases for PSi/c-Si due to the large value of leakage current coming from surface states.

The (I-V) characteristics of the heterojunctions at reverse bias under the illumination with white light as a function of light intensity are shown in Fig. 14. The photocurrent of GaN/PSi photodetector prepared at 532 nm is higher than that of GaN/PSi prepared at 1064 nm and PSi/c-Si photodetectors. This could be due to the large depletion width of GaN/Si prepared at 532 nm which comes from the large value of the carrier mobility. Increasing the light intensity leads to increases in the photocurrent of the photodetectors and no detectable saturation in photocurrent was observed after illumination with high light intensity indicating the quality of the linearity characteristics. [76–78].

Figure 15 presents the relationship of the squared reciprocal of the capacitance (C − 2) with the reverse voltage of GaN/PSi and PSi/c-Si heterojunctions. The linear relationship confirms that the fabricated heterojunctions are abrupt junctions. Moreover, the built-in potential value was determined by extrapolating the linear portion of the curve to the value of $1/C^2 = 0$ points. The estimated Vbi values were lower than the estimated values of the voltage turn-on from I-V properties due to the high electrical resistivity of gallium nitride nanostructures [79–81]. In addition, the value of the built-in potential of GaN/PSi prepared at 532 nm was larger than that of the other fabricated heterojunctions due to the large depletion width of a sample prepared at 532 nm.

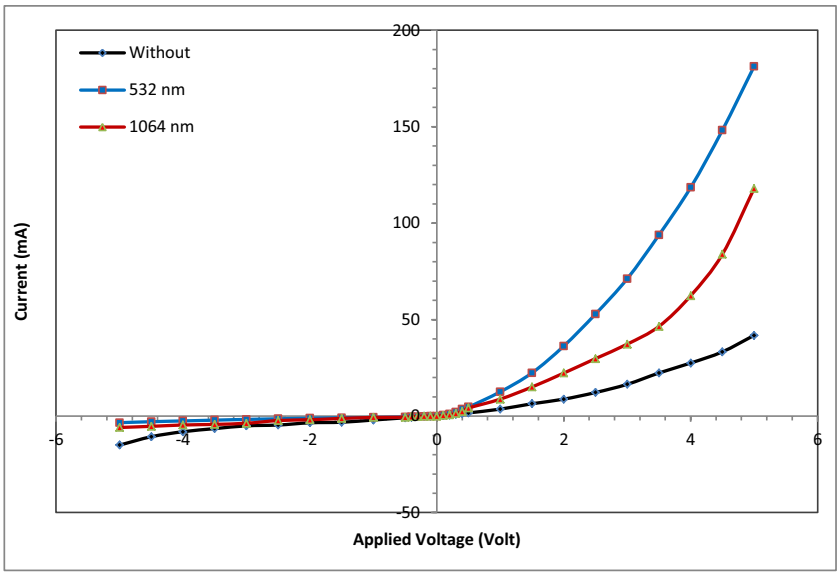

Fig. 13 I-V characteristic of porous silicon and GaN/PsSi photodetectors prepared at different laser wavelengths

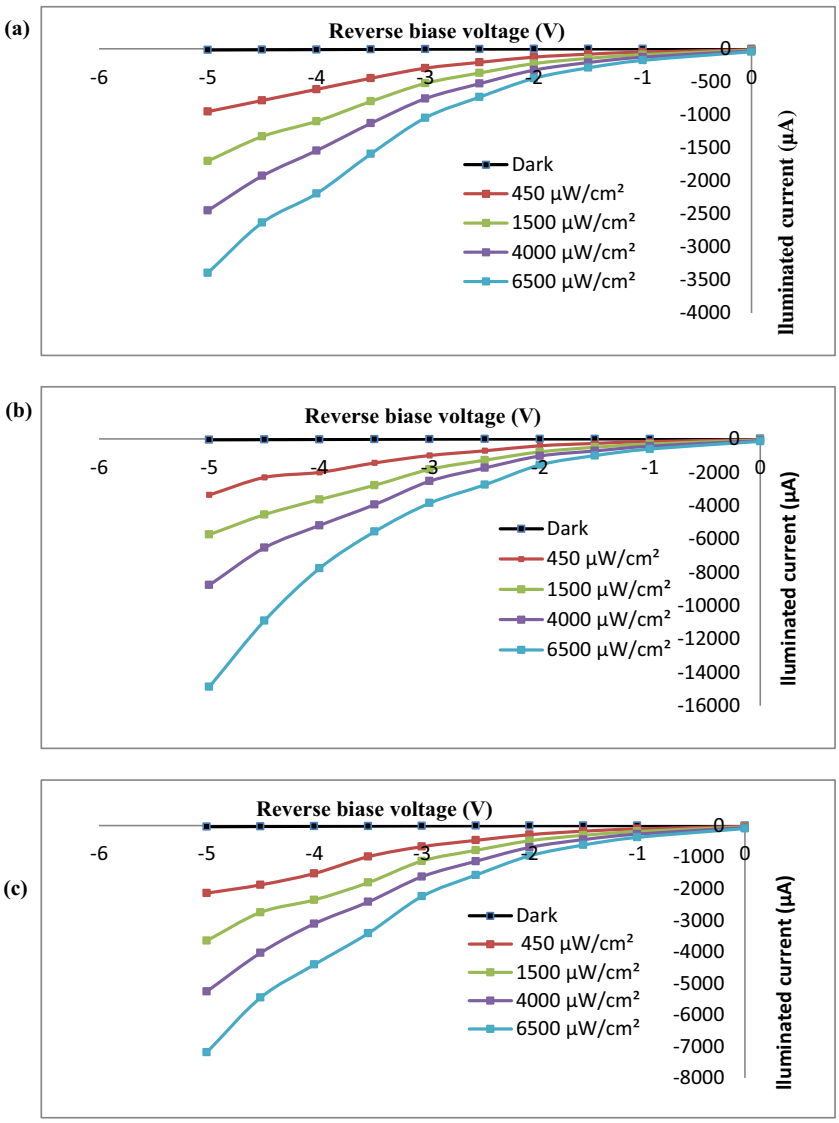

Fig. 14 Illuminated I-V of porous Silicon and GaN/PsSi photodetectors prepared at different laser wavelengths under the effect of different light intensities. (**a**) pSi substrates, (**b**) GaN/PsSi at wavelength of (532 nm) and (**c**) GaN/PsSi at wavelength of (1064 nm)

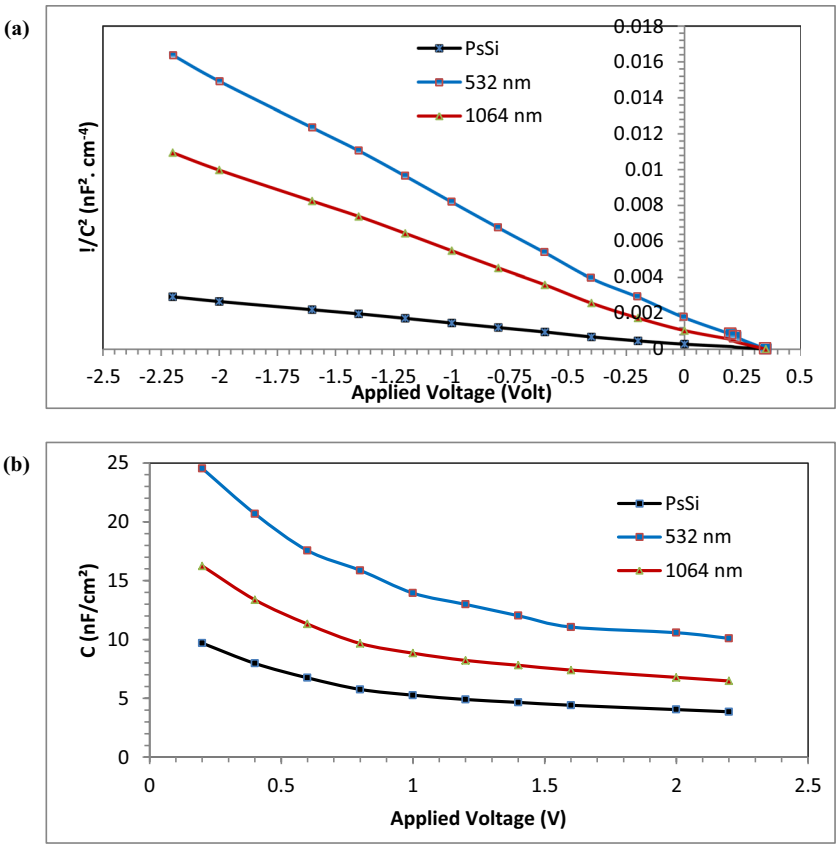

Fig. 15 Porous silicon and GaN/PsSi heterostructure at different laser ablation wavelengths of (**a**) $1/C^2$ as a function of the voltage and (**b**) C-V.

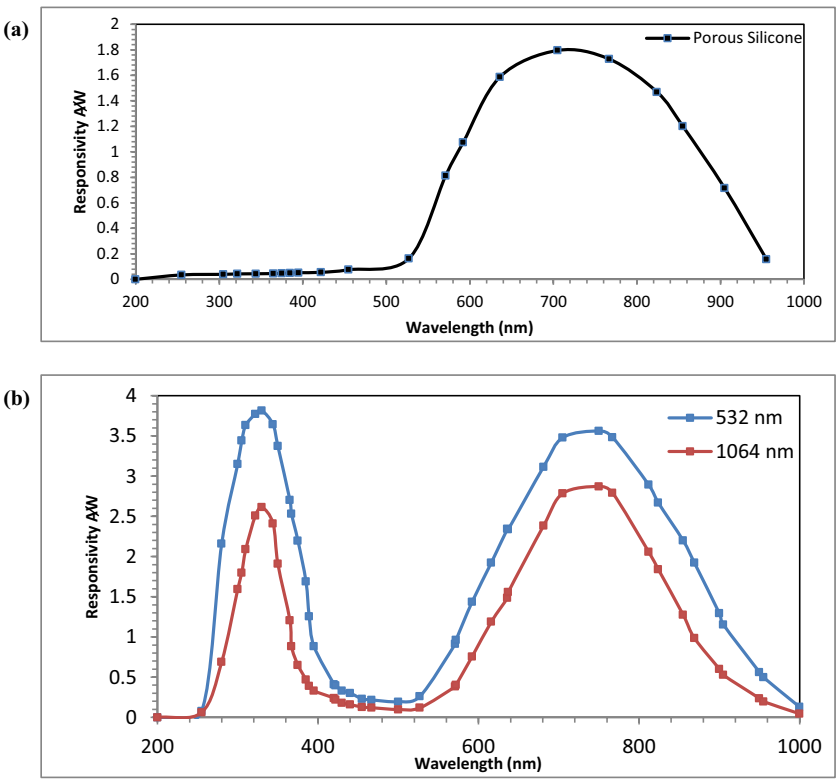

Fig. 16 Spectral responsivity of Porous Si and GaN/PsSi photodetectors fabricated at different laser wavelengths and 5 V bias

The spectral responsivity for the prepared porous Silicon and GaN/psSi heterostructure at the bias of 5 Volts is shown in Fig. 16. The spectral responsivity of the prepared porous silicon is presented in Fig. 16a; it shows a peak of 1.79 AW^{-1} at wavelength 705 nm [82–84]. Figure 16b presents the spectral responsivity for the gallium nitride nano heterostructure. In this figure, two prominent areas of the response have been identified. First ~ 330 nm for the nano gallium nitride and ~ 750 nm for the prepared nanoporous silicon wafer. The responsivity at 330 nm increased from 2.61 AW^{-1} to 3.81 AW^{-1} by reducing the ablation wavelength from 1064 to 532 nm. The increase in responsivity is a result of an increase in the width of the depletion region and the length of the diffusion. Increasing the efficiency of the carrier collection increases the absorption of the photons at the depletion region [85–87].

Figure 17 presents the specific detectivity D* of the GaN/psSi heterostructure. The detectivity values are influenced by the current noise and the spectral responsivity values [88–90], which were previously exhibited as a function of the pulsed laser wavelength. The values of the specific detectivity change with a value of the wavelengths precisely the same as in the values of the spectral responsivity. Figure 17a exhibits the specific detectivity of the prepared porous silicon; it shows a peak of 1.79×10^{14} W^{-1} cm $Hz^{0.5}$ at wavelength 705 nm. Figure 17b presented two peaks along the applied wavelengths. The 1064 nm pulsed laser wavelength, the value of the specific detectivity (2.61×10^{14} W^{-1} cm $Hz^{0.5}$ at the wavelength of 330 nm and 2.87×10^{14} W^{-1} cm $Hz^{0.5}$ at the wavelength of 750 nm), while decreasing the pulsed laser wavelength (using second harmonic generation) from 1064 to 532 nm will exhibit high-value of the specific detectivity (3.81×10^{14} W^{-1} cm $Hz^{0.5}$ at the wavelength of 330 nm and 3.56×10^{14} W^{-1} cm $Hz^{0.5}$ at the wavelength of 750 nm). Furthermore, the decrease in the values of the leakage current causes an increase in the detectivity of the photodetector. The fabricated photodetector and the result presented here can detect the UV signals and the weak Near-infrared signal.

The response time and the minority carrier lifetime for the prepared porous Silicon and GaN/psSi heterostructure at two laser wavelengths [(Fig. 18)]. The concept of carrier lifetime is to increase the absorption of light energy on the device surface by increasing internal voltage with the depletion layer employed to separate electron–hole pairs. The response time is the root mean square sum of the charge collection time. It is affected by the carrier drift time from the depletion layer, carrier diffusion time, and depletion layer capacitance

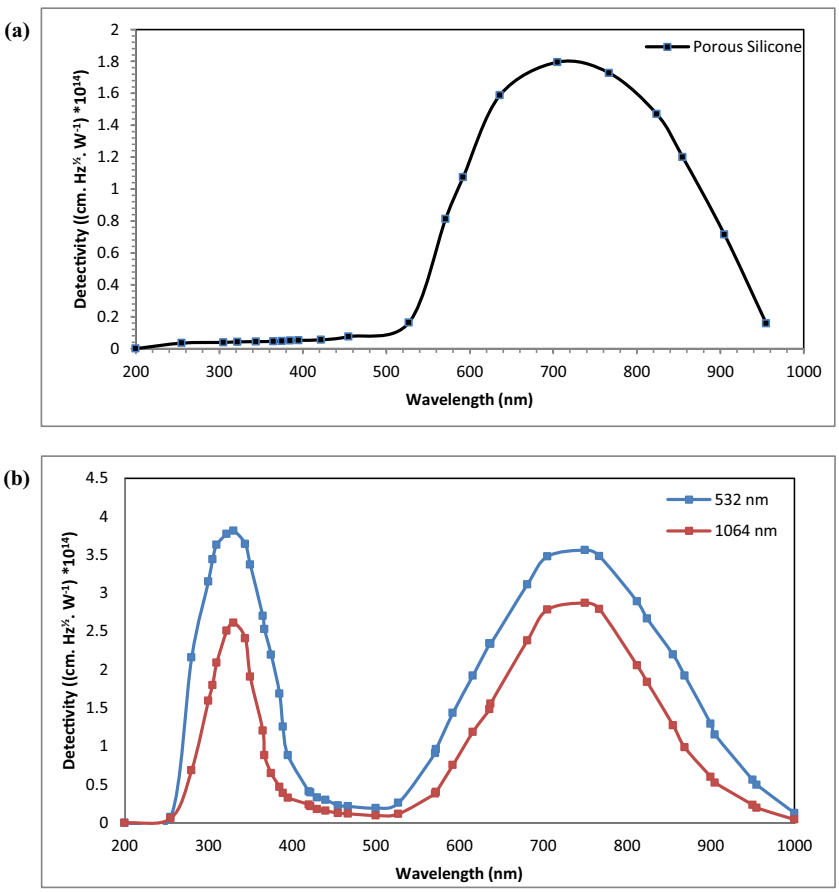

Fig. 17 Specific detectivity of Porous Si and GaN/PsSi photodetectors fabricated at different laser wavelengths and 5 V bias

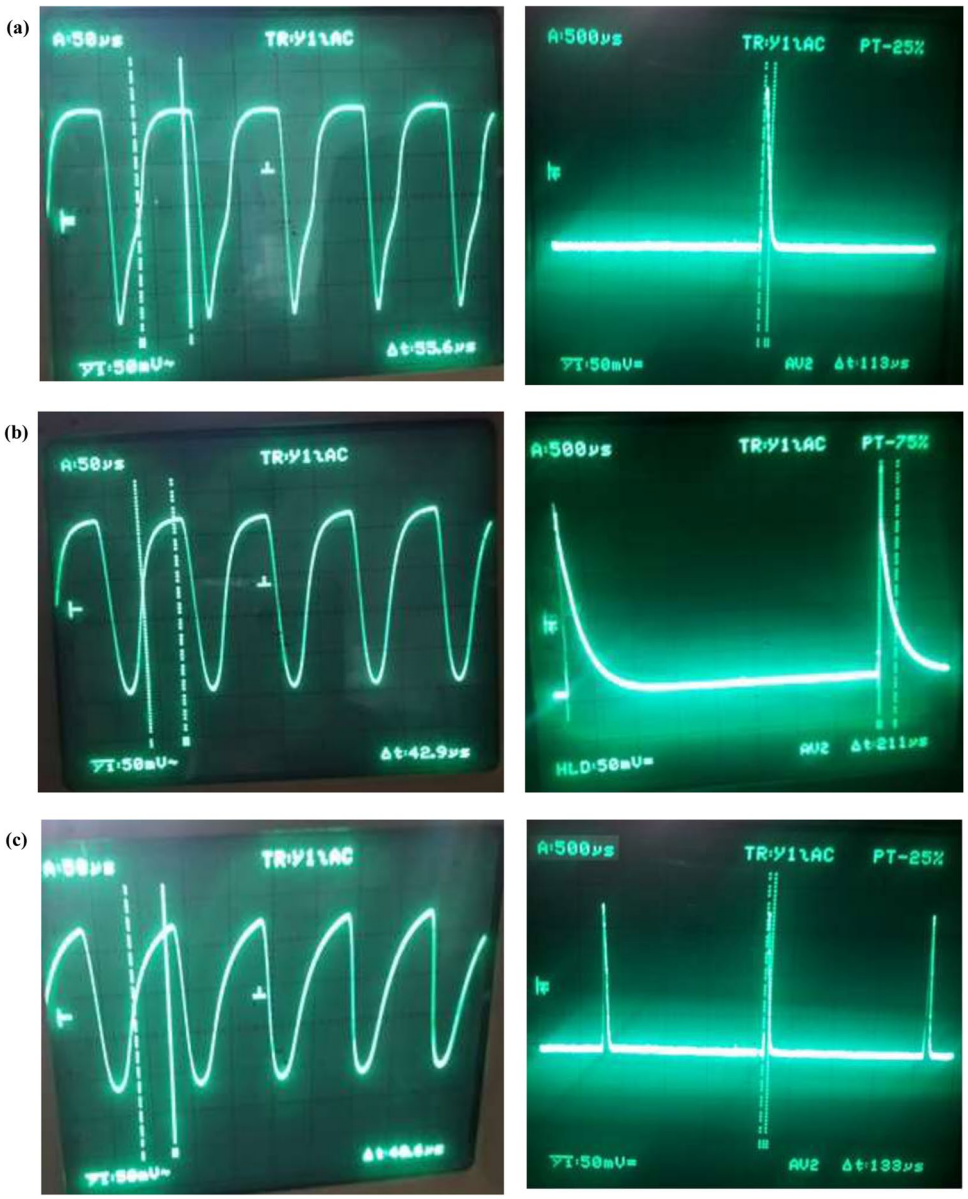

Fig. 18 Response time and the minority carrier lifetime of porous Silicon and GaN/PsSi photodetectors prepared at different laser wavelengths (**a**) psSi substrates, (**b**) GaN/PsSi at the wavelength of (532 nm), and (**c**) GaN/PsSi at the wavelength of (1064 nm)

Table 2 Response time and the minority carrier lifetime of porous Silicon and GaN/PsSi photodetectors prepared at different laser wavelengths

Type of substrate	Response time (μs)	minority carrier lifetime (μs)
psSi substrates	55.6	113
$(GaN/PsSi)_{532}$	42.9	211
$(GaN/PsSi)_{1064}$	48.6	133

[91, 92]. Figure 18a exhibits that the porous silicon has a Response time of 55.6 μs, and a minority carrier lifetime is 113 μs. Figure 18b presents the shortest Response time, 42.9 μs, and the highest minority carrier lifetime, 211 μs for GaN/psSi at wavelength 532 nm (using second harmonic generation). The Response time in Fig. 18c is 48.6 μs, and the minority carrier lifetime is 133 μs for GaN/psSi at wavelength 1064 nm. These results show that the response time decrease with decreasing laser ablation wavelength due to the optical generation of electron–hole pairs [93–95], all values of the Response time and minority carrier lifetime are tabulated in Table 2.

The scheme of the energy bundles of the fabricated double-junction device at the optimum conditions using the wavelength of the frequency doubling at the wavelength of 532 nm (second harmonic generation), and can be illustrated in the schematic form of the energy bundles (Fig. 19), where this scheme gives a greater indication of the mechanism of interaction of materials with each other and the energy

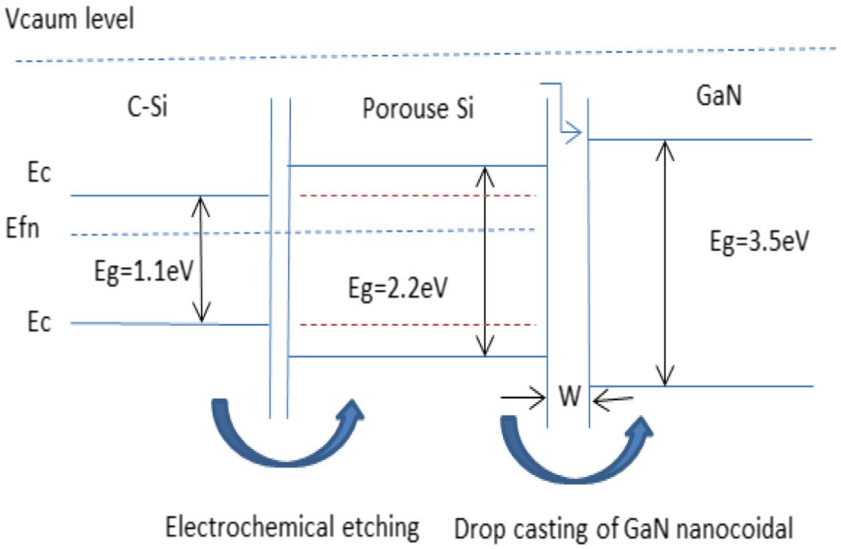

Fig. 19 The scheme of the energy bundles of the fabricated double-junction device at the optimum conditions

changes at the material contact area to form heterogeneous hybrid separators [92–95].

4 Conclusion

A High-performance GaN/PSiSi heterojunction photodetector was successfully prepared using a simple and low-cost PLAL technique. As the laser ablation wavelength decreases, the bandgap value of the deposited Nano GaN films increases. GaN nano-films created at low laser wavelengths exhibited a shift that towered over the blue region. The device performance results established two response peaks at 330 nm, and 750 nm, GaN/psSi sample for wavelength 532 nm shows a higher responsivity peak of 3.81 AW^{-1} than the sample of 1064 nm due to the increase in the width of the depletion region and the length of the diffusion, increasing the efficiency of the carrier collection, increasing the absorption of the photons at the region of the depletion. The shortest response time was 42.9 µs, and the highest minority carrier lifetime was 211 µs for GaN/psSi that was prepared at wavelength 532 nm due to the optical generation of electron–hole pairs. The high Ultra-Violet response of the manufactured devices (photodetectors) indicates that the technology used here is encouraging and prospective for producing Ultra-Violet detectors that are both cost-effective and simple.

Acknowledgements The authors would like to thank the University of Technology for the logistic support this work.

Author Contributions Makram A. Fakhri, Ali. A.Alwahib, Evan T. Salim, Raid A. Ismail, Husam Aldin A. Abdul Amir, Raed Khalid Ibrahim, Sarmad Fawzi Hamza Alhasan, Forat H. Alsultany, Zaid T. Salim, Subash C.B. Gopinath Conceptualization, Makram A. Fakhri, Ali. A.Alwahib and Evan T. Salim; methodology, Makram A. Fakhri, Evan T. Salim, and Husam Aldin A. Abdul Amir; software, Makram A. Fakhri, Ali. A.Alwahib and Husam Aldin A. Abdul Amir; validation, Makram A. Fakhri, Evan T. Salim, and Ali. A. Alwahib; formal analysis, Makram A. Fakhri, Evan T. Salim, and Husam Aldin A. Abdul Amir; investigation, Makram A. Fakhri, Evan T. Salim, Husam Aldin A. Abdul Amir, and U. Hashim; resources, Makram A. Fakhri, Evan T. Salim, and Husam Aldin A. Abdul Amir; data curation, Makram A. Fakhri, Evan T. Salim, and Husam Aldin A. Abdul Amir; writing—original draft preparation, Ali. A. Alwahib, and Husam Aldin A. Abdul Amir; writing—review and editing, Makram A. Fakhri, Evan T. Salim, and Ali. A. Alwahib, Subash C.B. Gopinath; visualization, Makram A. Fakhri, Evan T. Salim, Raed Khalid Ibrahim, Sarmad Fawzi Hamza Alhasan, Forat H. Alsultany, Zaid T. Salim, and Subash C.B. Gopinath; supervision, Makram A. Fakhri, Ali. A. Alwahib, and Evan T. Salim; project administration, Makram A. Fakhri, Evan T. Salim, Ali. A. Alwahib, Raed Khalid Ibrahim, Sarmad Fawzi Hamza Alhasan, and U. Hashim; funding acquisition, Makram A. Fakhri, Evan T. Salim, and Husam Aldin A. Abdul Amir, All authors have read and agreed to the published version of the manuscript.

Data Availability Correspondence and requests for materials should be addressed to M.A. Fakhri, and E. T. Salim.

Declarations

Competing interests The authors declare no competing interests.

Consent for Publication Not applicable.

Conflicts of Interest We hereby confirm that the authors have no conflict of interest and the disclosure made for this manuscript is complete and correct to the best of our information and belief. We agree that if we become aware of any information that might indicate that this disclosure is inaccurate or that we have not complied with the conflict of interest policy, we will notify the journal immediately.

References

1. Song H, Lee S (2007) Red light emitting solid state hybrid quantum dot–near-UV GaN LED devices. Nanotechnology 18(25):255202

2. Ikawa Y, Lee K, Ao J-P, Ohno Y (2014) Two-dimensional device simulation of AlGaN/GaN heterojunction FET side-gating effect. Jpn J Appl Phys 53(11):114302
3. Jabbar HD, Fakhri MA, Abdulrazzaq MJ (2021) Gallium Nitride -Based Photodiode: A review. Mater Today: Proceedings 42:2829–2834
4. Podolska A, Seeber RM, Mishra UK, Pfleger KDG, Parish G, Nener BD (2012) Detection of biological reactions by AlGaN/GaN biosensor. Commad 2012:75–76
5. Abdul Amir HAA, Fakhri MA, Alwahib AA (2021) Review of GaN optical device characteristics, applications, and optical analysis technology. Mater Today: Proceedings 42:2815–2821
6. Khan MAH, Rao MV, Li Q (2019) Recent advances in electrochemical sensors for detecting toxic gases: NO2, SO2 and H2S. Sensors 19(4):905
7. Prokopuk N, Son K-A, George T, and Moon JS, (2005) Development of GaN-based micro chemical sensor nodes, Sensors, 20045 IEEE, Irvine. https://doi.org/10.1109/ICSENS.2005.1597670
8. Abdul-Hamead AA, Othman FM, Fakhri MA (2021) Preparation of MgO–MnO2 nanocomposite particles for cholesterol sensors. J Mater Sci: Mater Electron 32:15523–15532
9. Pearton SJ, Kang BS, Kim S, Ren F, Gila BP, Abernathy CR, Lin J, Chu SNG (2004) GaN-based diodes and transistors for chemical, gas, biological and pressure sensing. J Phys Condens Matter 16(29):R961
10. Monroy E, Muñoz E, Sánchez FJ, Calle F, Calleja E, Beaumont B, Gibart P, Muñoz JA, Cussó F (1998) High-performance GaN pn junction photodetectors for solar ultraviolet applications. Semicond Sci Technol 13(9):1042
11. Amir HAAA, Fakhri MA, Alwahib AA, Salim ET, Alsultany FH, Hashim U (2022) Synthesis of gallium nitride nanostructure using pulsed laser ablation in liquid for photoelectric detector. Mater Sci Semicond Process 150:106911
12. Jabbar HD, Fakhri MA, Razzaq MJA, Dahham OS, Salim ET, Alsultany FH (2023) Effect of different etching time on fabrication of an optoelectronic device based on GaN/Psi. J Renew Mater 11(3):1101–1122. https://doi.org/10.32604/jrm.2023.023698
13. Mosca M, Reverchon J-L, Grandjean N, Duboz J-Y (2004) Multilayer (Al, Ga) N structures for solar-blind detection. IEEE J Sel Top Quantum Electron 10(4):752–758
14. Biyikli N, Kimukin I, Aytur O, Ozbay E (2004) Solar-blind AlGaN-based pin photodiodes with low dark current and high detectivity. IEEE Photonics Technol Lett 16(7):1718–1720
15. Abbar HD, Fakhri MA, AbdulRazzaq MJ (2022) Synthesis gallium nitride on porous silicon nano-structure for optoelectronics devices. Silicon 14(18):12837–1285. https://doi.org/10.1007/s12633-022-01999-8
16. Biyikli N, Kimukin I, Tut T, Kartaloglu T, Aytur O, Ozbay E (2004) High-speed characterization of solar-blind AlxGa1− xN p–i–n photodiodes. Semicond Sci Technol 19(11):1259
17. Parish G et al (1999) High-performance (Al, Ga) N-based solar-blind ultraviolet p–i–n detectors on laterally epitaxially overgrown GaN. Appl Phys Lett 75(2):247–249
18. Amir HAAA, Fakhri MA, Alwahib AA, Salim ET, Alsultany FH, Hashim U (2022) An investigation on GaN/ porous-Si NO2 gas sensor fabricated by pulsed laser ablation in liquid. Sensors Actuators B: Chem 367:132163
19. Osinsky A et al (1997) Low noise p-π-n GaN ultraviolet photodetectors. Appl Phys Lett 71(16):2334–2336
20. Adivarahan V et al (2000) SiO 2-passivated lateral-geometry GaN transparent Schottky-barrier detectors. Appl Phys Lett 77(6):863–865
21. Abdul Amir HAA, Fakhri MA, Alwahib AA, Salim ET (2022) Optical Investigations of GaN Deposited Nano Films Using Pulsed Laser Ablation in Ethanol. Int J Nanoelectron Mater 15(2):129–138
22. Chang S-J et al (2003) GaN metal-semiconductor-metal photodetectors with low-temperature-GaN cap layers and ITO metal contacts. IEEE Electron Device Lett 24(4):212–214
23. Katz O, Garber V, Meyler B, Bahir G, Salzman J (2001) Gain mechanism in GaN Schottky ultraviolet detectors. Appl Phys Lett 79(10):1417–1419
24. Salim ET, Khalid FG, Fakhri MA, Mahmood RS (2021) Laser wavelength effects on the optical, structure, and morphological properties of nano HfO2structures. Mater Today: Proceedings 42:2422–2425
25. Monroy E, Palacios T, Hainaut O, Omnes F, Calle F, Hochedez J-F (2002) Assessment of GaN metal–semiconductor–metal photodiodes for high-energy ultraviolet photodetection. Appl Phys Lett 80(17):3198–3200
26. Pau JL et al (2004) Response of ultra-low dislocation density GaN photodetectors in the near-and vacuum-ultraviolet. J Appl Phys 95(12):8275–8279
27. Fakhri MA, Razzaq MJA, Jabbar HD, Salim ET, Alsultany FH, Hashim U (2023) Fabrication of UV photodetector based on GaN/Psi heterojunction using pulse laser deposition method: Effect of different laser wavelengths. Opt Mater 137:113593
28. Ishikawa H, Shimanaka K, Azfar Bin M, Amir M, Hara Y, Nakanishi M (2010) Improved MOCVD growth of GaN on Si-on-porous-silicon substrates. Phys Status Solidi C 7(7–8):2049–2051
29. Dadgar A et al (2007) Epitaxy of GaN on silicon—impact of symmetry and surface reconstruction. New J Phys 9(10):389
30. Fakhri Makram A, Salim Evan T, Abdulwahhab Ahmed W, Hashim U, Minshid Mohammed A, Salim Zaid T (2019) The Effect of Annealing Temperature on Optical and Photolumence Properties of LiNbO 3. Surf Rev Lett 26(10):1950068
31. Manna S, Ashok VD, De SK (2010) Rectifying properties of p-GaN nanowires and an n-silicon heterojunction vertical diode. ACS Appl Mater Interfaces 2(12):3539–3543
32. Tang Y et al (2008) Controllable Synthesis of Vertically Aligned p-Type GaN Nanorod Arrays on n-Type Si Substrates for Heterojunction Diodes. Adv. Funct Mater 18(21):3515–3522
33. Salim Evan T (2012) Rapid thermal oxidation for silicon nanocrystal based solar cell. Int J Nanoelectron Mater 5(2):95–100
34. Xu Z, Zhang L, He H, Wang J, Xie M (2011) Growth of GaN on Si (111): Surfaces and crystallinity of the epifilms and the transport behavior of GaN/Si heterojunctions. J Appl Phys 110(9):93514
35. Nabi G et al (2012) Synthesis, photoluminescence and field emission properties of well aligned/well patterned conical shape GaN nanorods. Cryst Eng Comm 14(24):8492–8498
36. Fakhri MA, Salim ET, Tariq SM, Ibrahim RK, Alsultany FH, Alwahib A A, Alhasan SFH, Gopinath SCB, Salim ZT, Hashim U (2023) A gold nanoparticles coated unclad single mode fiber-optic sensor based on localized surface plasmon resonance. Sci Rep 13:5680. https://doi.org/10.1038/s41598-023-32852-6
37. Goodwin TJ, Leppert VJ, Risbud SH, Kennedy IM, Lee HWH (1997) Synthesis of gallium nitride quantum dots through reactive laser ablation. Appl Phys Lett 70(23):3122–3124
38. Mohapatra S, Nguyen TA, and Nguyen-Tri P (2018) Noble metal-metal oxide hybrid nanoparticles: fundamentals and applications, Elsevier 8:157–178. https://doi.org/10.1016/C2017-0-00847-9
39. Naayi SA, Hassan AI, Salim ET (2018) FTIR and X-ray diffraction analysis of Al2O3nanostructured thin film prepared at low temperature using spray pyrolysis method. Int J Nanoelectron Mater 11(Special Issue BOND21):1–6
40. Qaeed MA, Ibrahim K, Saron KMA, Salhin A (2013) Cubic and hexagonal GaN nanoparticles synthesized at low temperature. Superlattices Microstruct 64:70–77
41. Salim ET, Ismail RA, Halbos HT (2020) Deposition geometry effect on structural, morphological and optical properties of

Nb2O5 nanostructure prepared by hydrothermal technique. Appl Phys A 126:891
42. Sudhir GS et al (1998) Control of the structure and surface morphology of gallium nitride and aluminum nitride thin films by nitrogen background pressure in pulsed laser deposition. J Electron Mater 27(4):215–221
43. Salim Evan T, Al-Wazny Marwa S, Fakhri Makram A (2013) Glancing angle reactive pulsed laser deposition (GRPLD) for Bi 2O3/Si heterostructure. Modern Physics Lett B 27(16):1350122
44. Ismail Raid A, Rasheed Bassam G, Salm Evan T, Al-Hadethy Mukram (2007) High transmittance-low resistivity cadmium oxide films grown by reactive pulsed laser deposition. J Mater Sci: Mater Electron 18(10):1027–1030
45. Mantarcı A (2020) Structural, Morphological, and Optical Characterization of GaN/p-Si Thin Films for Various Argon Flow Rates. JOM 72(1):552–560
46. Ajimsha RS, Jayaraj MK, Kukreja LM (2008) Electrical characteristics of n-ZnO/p-Si heterojunction diodes grown by pulsed laser deposition at different oxygen pressures. J Electron Mater 37(5):770–775
47. Salim ET, Saimon JA, Abood MK, Fakhri MA (2019) Electrical conductivity inversion for Nb2O5 nanostructure thin films at different temperatures. Mater Res Express 6(12):126459
48. Mondal P, Appani SK, Sutar DS, Major SS (2021) High performance GZO/p-Si heterojunction diodes fabricated by reactive co-sputtering of Zn and GaAs through the control of GZO layer thickness. RSC Adv 11(32):19779–19787
49. Ismail RA (2010) Fabrication and characterization of photodetector based on porous silicon. e-J Surf Sci 8:388–391
50. Muhammed QQ, Saleh MM, Al-Azawi RJ, Kadhim AC, Shaker RM (2022) Close-Range photogrammetric techniques for investigating and documenting. In: The ancient buildings, optics info base conference papers, p JTu5A.91. https://doi.org/10.1364/FIO.2022.JTu5A.91
51. Fakhri MA, Salim Evan T, Wahid MHA, Abdulwahhab Ahmed W, Hashim U, Salim Zaid T (2019) Efficiency enhancement of optical strip waveguide by the effect of heat treatment. Optik 180:768–774
52. Salim ET, Hassan AI, Mohamed FA, Wahid MHA, Fakhri MA (2023) A sight of view on electrical impacts, structural properties and surface roughness of tungsten trioxide thin film: effect of substrate temperatures in WO3/Si device fabrication. Physica Scripta 98(3):035508
53. Zhu P, Seifert HJ, Pfleging W (2019) The ultrafast laser ablation of Li (Ni0. 6Mn0. 2Co0. 2) o2 electrodes with high mass loading. Appl Sci 9(19):4067
54. Fakhri MA, Salim Evan T, Wahid MHA, Hashim U, Salim Zaid T (2018) Optical investigations and optical constant of nano lithium niobate deposited by spray pyrolysis technique with injection of Li2CO3and Nb2O5 as raw materials. J Mater Sci: Mater Electron 29(11):9200–9208
55. Ismail RA, Fadhil FA (2014) Effect of electric field on the properties of bismuth oxide nanoparticles prepared by laser ablation in water. J Mater Sci: Mater Electron 25:1435–1440
56. Fakhri MA, Salim Evan T, Hashim U, Abdulwahhab Ahmed W, Salim Zaid T (2017) Annealing temperature effect on structural and morphological properties of nano photonic LiNbO3. J Mater Sci: Mater Electron 28(22):16728–16735
57. Tulej M et al (2021) Current Progress in Femtosecond Laser Ablation/Ionisation Time-of-Flight Mass Spectrometry. Appl Sci 11(6):2562
58. Fakhri MA, Basheer RA, Banoosh AM, and Azeez HN (2021) Rapid thermal oxidation of nano silver film for solar cell fabrication. Dig J Nanomater Biostructures 16(2):367–375
59. Shafeeq SR, Abdul Razzaq MJ, Salim ET, Wahid MH (2022) Significance of niobium (v) oxide for practical applications: a review. Key Eng Mater 911:89–95
60. Kim K-S, Chung G-S (2011) Characterization of porous cubic silicon carbide deposited with Pd and Pt nanoparticles as a hydroge sensor. Sens Actuators B Chem 157:482–487
61. Fakhri Makram A, Salim Evan T, Wahid MHA, Hashim U, Salim Zaid T, Ismail Raid A (2017) J Mater Sci: Mater Electron 28(16):11813–11822
62. Evan T (2013) Salim, Optoelectronic properties of Fe2O3/Si heterojunction prepared by rapid thermal oxidation method. Indian J Physics 87(4):349–353
63. Kung P et al (1995) Kinetics of photoconductivity in n-type GaN photodetector. Appl Phys Lett 67(25):3792–3794
64. Urich A, Unterrainer K, Mueller T (2011) Intrinsic response time of graphene photodetectors. Nano Lett 11(7):2804–2808
65. Salim Evan T, Agool Ibrahim R, Muhsien Marwa A (2011) Construction of SnO2/SiO2/Si heterojunction and its lineup using I-V and C-V measurements. Int J Modern Physics B 25(29):3863–3869
66. Ismail RA, Yehya KZ, Abdulrazaq OA (2005) Preparation and photovoltaic properties of Ag2O/Si isotype heterojunction. Surf Rev Lett 12:299–303
67. Fakhri MA, Al-Douri Y, Salim ET, Hashim U, Yusof Y, Choo EB, Salim ZT, Jurn YN (2016) Structural properties and surface morphology analysis of nanophotonic LINBO3. ARPN J Eng Appl Sci 11(8):4974–4978
68. Hashim AH, Jasim OZ, Salih MM (2022) The Establishing of Geospatial Database for Agricultural Lands of Islamic WAQF in Iraq: Case Study Babil Province. IOP Conf Series: Earth Environ Sci 961(1):012025
69. Abood MK, Halim M, Wahid A, Salim ET, Admon Jehan (2017) Niobium Pentoxide thin films employ simple colloidal suspension at low preparation temperature. Eur Physical J Conf 162(12):01058
70. Sultan FI, Slman AA, Nayef UMJE, Journal T (2013) IV and CV characteristics of porous silicon nanostructures by electrochemical etching. Eng Tech J 3(31):332–338
71. Al Wazny MS, Salim ET, Bader BA, Fakhry MA (2018) Bi2O3 films, studying their optical, structural, and surface roughness properties. IOP Conf Series Mater Sci Eng 454(1):012160
72. Pujadó MP (2012) Carbon nanotubes as platforms for biosensors with electrochemical and electronic transduction. Springer Theses, Springer Berlin, Heidelberg. https://doi.org/10.1007/978-3-642-31421-6
73. Evan T (2013) Salim, Surface morphology and X-ray diffraction analysis for silicon nanocrystal-based heterostructures. Surf Rev Lett 20(05):1350046
74. Jasim Farah Z, Abdul-Razzak Mohammed J, Ahmed Hisham M (2014) Design of GaN-based VCSEL with high performance. Ootoelectron Adv Mater-Rapid Commun 8(1–2):7–9
75. Muhammad YS, Ijaz H, Nargis B, Esteban B, Omer N et al (2012) Nanoscale elastic modulus of single horizontal ZnO nanorod using nanoindentation experiment. Nanoscale Res Lett 7(146):1–5
76. Abd AN, Habubi NF, Reshak AH, Mansour HN (2018) Enhancing the electrical properties of porous silicon photodetector by depositing MWCNTs. Int J Nanoelectron Mater 11(3):241–248
77. AbdulRazzaq MJ, Shibib KS, Younis SI (2020) Temperature distribution and stress analysis of end pumped lasers under Gaussian pump profile. Opt Quant Electron 52:379
78. Fakhri MA, Numan NH, Mohammed QQ, Abdulla MS, Hassan OS, Abduljabar SA, Ahmed AA (2018) Responsivity and response time of nano silver oxide on silicon heterojunction detector. Int J Nanoelectron Mater 11(Special Issue BOND21):109–114

79. Ismail Raid A, Khashan Khawla S, Alwan Alwan M (2017) Study of the Effect of Incorporation of CdS Nanoparticles on the porous silicon photodetector. Silicon 9:321–326
80. Abood MK, Salim ET, Saimon JA (2018) Impact of substrate type on the microstructure of H-Nb2o5 thin film at room temperature. Int J Nanoelectron Mater 11(Special Issue BOND21):55–64
81. Wright AF, Nelson JS (1995) Consistent structural properties for AlN, GaN, and InN. Phys Rev B 51(12):7866
82. Fakhri MA, Numan NH, Mohammed QQ, Abdulla MS, Hassan OS, Abduljabar SA, Ahmed AA (2018) Responsivity and response time of nano silver oxide on silicon heterojunction detector. Int J Nanoelectron Mater 11(Special Issue BOND21):65–72
83. Hannun RM, Salih MM (2019) Converting Zubair oil field permanent power generation from single cycle into combined-cycle with plant exergy analysis. J Physics: Conf Series 1279(1):012058
84. Mantarcı A, Kundakci M (2020) Production of GaN/n–Si thin films using RF magnetron sputtering and determination of some physical properties: argon flow impacts. J Aust Ceram Soc 56(3):905–914
85. Ben Nasr F, Guermazi H, Guermazi S (2016) Correlation between structural and optical properties of GaN epi-layers by the cathodoluminescence technique. Eur Phys J Plus 131(6):1–7
86. Al-Douri Y, Fakhri MA, Badi N, Voon CH (2018) Effect of stirring time on the structural parameters of nanophotonic LiNbO3 deposited by spin-coating technique. Optik 156:886–890
87. Al-Douri Y, Fakhri Makram A, Bouhemadou A, Khenata R, Ameri M (2018) Stirrer time effect on optical properties of nanophotonic LiNbO3. Mater Chem Physics 203:243–248
88. Abdul Muhsien M, Salim ET, Al-Douri Y, Sale AF, Agool IR (2015) Synthesis of SnO2 nanostructures employing Nd:YAG laser. Appl Physics A 120(2):725–730
89. Ravi L, Boopathi K, Panigrahi P, Krishnan B (2018) Growth of gallium nitride nanowires on sapphire and silicon by chemical vapor deposition for water splitting applications. Appl Surf Sci 449:213–220
90. Fakhri Makram A, Hashim U, Salim Evan T, Salim Zaid T (2016) Preparation and charactrization of photonic LiNbO3generated from mixing of new raw materials using spry pyrolysis method. J Mater Sci: Mater Electron 27(12):13105–13112
91. Ismail RA, Habubi NF, Abbod MM (2016) Preparation of high-sensitivity In2S3/Si heterojunction photodetector by chemical spray pyrolysis. Opt Quantum Electron 48:1–14
92. Ee YL, Biser X, Cao J, Chan W, Vinci HM, Tansu RP (2010) Abbreviated MOVPE nucleation of III-nitride light-emitting diodes on nano-patterned sapphire. J Cryst Growth 312(8):1311–1315
93. Mahdi Rana O, Fakhri Makram A, Salim Evan T (2020) physical investigations of niobium oxide nanorod imploring laser radiation. Mater Sci Forum 1002:211–220
94. Qi WH, Huang BY, Wang MP, Yin ZM, Li J (2008) Shape factor for non-cylindrical nanowires. Phys B Condens Matter 403(13–16):2386–2389
95. He XG, Zhao DG, Jiang DS, Zhu JJ, Chen P, Liu ZS, Le LC, Yang J, Li XJ, Liu JP, Zhang LQ, Yang H (2016) GaN high electron mobility transistors with AlInN back barriers. J Alloys Compd 662:16–19